Published in final edited form as:
Magn Reson Med. 2010 March ; 63(3): 658–666. doi:10.1002/mrm.22311.

Quantitative Analysis of Hyperpolarized ^{3}He Ventilation Changes in Mice Challenged with Methacholine

Nilesh N. Mistry[1,2], **Abraham Thomas**[2], **Sivaram Kaushik**[1,2], **G. Allan Johnson**[1,2], and **Bastiaan Driehuys**[1,2]

[1]Department of Biomedical Engineering, Duke University, Durham, NC

[2]Center for In Vivo Microscopy, Department of Radiology, Duke University Medical Center, Durham, NC

Abstract

The capability to use high-resolution ^{3}He MRI to depict regional ventilation changes and airway narrowing in mice challenged with methacholine (MCh) offers the opportunity to gain new insights into the study of asthma. However, to fully exploit the value of this novel technique, it is important to move beyond visual inspection of the images towards automated and quantitative analysis. To address this gap, we describe a post-processing approach to create ventilation difference maps to better visualize and quantify regional ventilation changes before and after MCh challenge. We show that difference maps reveal subtle changes in airway caliber, and highlight both focal and diffuse regional alterations in ventilation. Ventilation changes include both hypoventilation, as well as compensatory areas of hyperventilation. The difference maps can be quantified by a histogram plot of the ventilation changes, in which the standard deviation increases linearly with MCh dose (R^2=0.89). This method of analysis is shown to be more sensitive than simple threshold-based detection of gross ventilation defects. With suitable extension, this method should be useful in studies of both mice and human subjects.

Keywords

quantitative ventilation; hyperpolarized ^{3}He; mouse lung imaging; asthma; methacholine

INTRODUCTION

Recently, we demonstrated the capability to create high-resolution ^{3}He MR images in mouse models of asthma (1) before and after challenge with methcaholine (MCh). MCh administration causes regional changes in ventilation and airway caliber that are revealed by ^{3}He magnetic resonance imaging (MRI). In preliminary studies, mice were treated with a conventional ovalbumin-sensitization protocol (2) and then imaged before and after MCh challenge. These mice showed significant regional airway narrowing and closure (1) relative to non-sensitized control mice. This preliminary work suggests that ^{3}He MRI could ultimately offer new insights into the airway biology of asthma models compared to conventional global metrics, such as airway resistance (3,4) and bronchoalveolar lavage (5,6). Compared to these metrics, ^{3}He MRI promises to reveal spatially resolved differences in airways hyperresponsiveness (AHR) among sensitized mice that have been treated with a variety of therapeutic compounds.

Corresponding Author: Bastiaan Driehuys, PhD, Center for In Vivo Microscopy, Box 3302 Duke University Medical Center, Durham, NC 27710, 919 684-7786, (FAX) 919 684-7158, bastiaan.driehuys@duke.edu.

However, using ^{3}He MRI for such investigations requires the ability to generate quantitative measures from the images.

Quantitative analysis of hyperpolarized (HP) ^{3}He ventilation images is in its infancy. Clinical ^{3}He MR images have been analyzed by counting ventilation defects manually and assigning mean defects scores to each patient (7–9). Such methods, while representing important initial steps, are subjective and are not geared to a pixel-by-pixel analysis. One approach to make image analysis more objective and automated is to apply a simple threshold to count the number of pixels that are classified as ventilated versus unventilated. This idea was illustrated by Woodhouse *et al.* (10) and was useful in our initial work (1) for quantifying focal reduction in ventilation (for example: if the upper right lobe was completely unventilated). However, such methods fall short by applying only a binary mask (ventilated or unventilated), whereas regional pulmonary ventilation is known to have a far greater dynamic range (11).

To more quantitatively capture regional ventilation by ^{3}He MRI, a technique was introduced to determine the fraction of ^{3}He *r* replenished in each voxel with every breath (11). However, this method requires multiple HP ^{3}He images to be acquired, and delivering monotonically increasing numbers of breaths, while also accounting for signal depolarization over time. Thus, although this technique represents an important step towards quantification, it consumes large quantities of HP ^{3}He, takes considerable time, and produces ventilation maps with limited spatial resolution (~5 mm^3 in rodents).

Hypolarized ^{3}He MRI studies, before and after MCh challenge, offer an opportunity to simplify quantitative image analysis because the subjects act as their own control. Since images are taken at baseline and after challenge, it should be feasible to identify ventilation changes by simply subtracting the post-MCh images from the pre-MCh set. However, such subtraction is complicated by several factors—differences in gas volume inhaled, the possibility of patient movement during the time between the two images, and different levels of polarization pre- and post-intervention. Fortunately, some of these issues are mitigated in ^{3}He MRI of the mouse compared to clinical imaging. The mouse is anesthetized during imaging, and thus is not repositioned between baseline and post-MCh imaging. Furthermore, the mouse is mechanically ventilated and therefore does not alter its respiratory pattern between scans. Hence, the mouse system of MCh challenge and ^{3}He MRI represents an excellent test-bed for quantitative analysis of induced ventilation changes.

Despite these simplifying features, analysis of ^{3}He MR imaging of MCh challenge in the mouse is still confounded by several factors. First, despite the use of a constant volume ventilator, there can be some residual variability in gas volume delivered during pre- and post-MCh imaging. Second, signal differences can arise from different levels of polarization pre- and post-MCh challenge. Furthermore, although subject movement is not nearly as significant as for human scanning, millimeter changes in position can occur before and after MCh challenge, particularly when significant time elapses between baseline and post-MCh scans. Therefore, the image analysis technique must overcome these variables. In addition to dealing with these technical issues, the analysis should be capable of revealing the key features of altered ventilation that are hallmarks of the MCh challenge study—changes in airway caliber, focal ventilation changes, and diffuse ventilation changes (1).

In this paper, we outline a process needed to generate quantitative ventilation difference maps that consists of four steps: 1) correct the images using automated image registration to account for motion or shape changes in the pre- and post-MCh images; 2) normalize the images to compensate for non-physiological factors that may cause global signal intensity changes between the pre- and post-MCh studies; 3) subtract the registered and normalized pre- and post-MCh images to generate a difference map; 4) quantify the difference map. To this end,

we generate its histogram and use the standard deviation of the difference map histogram as a quantitative biomarker to study the heterogeneity of response to different treatments. We show that the standard deviation of the difference map increases linearly with MCh dose.

METHODS

Studies

All aspects of the animal welfare and experimentation were approved by the Duke University Institutional Animal Care and Use Committee. Salient details of the animal handling for imaging are provided in references (1,12). Of particular relevance to this work are the following details. For some studies, mice were sensitized and challenged with ovalbumin as outlined in (12) to cause their airways to become hyperresponsive to MCh challenge. For all imaging studies, mice were intubated with an 18G catheter (Hospira, Inc., Lake Forest, IL, USA) and mechanically ventilated at 100 breaths per minute, with each cycle consisting of a 240 ms inspiration, 100 ms breath-hold, and 260 ms exhalation period. The ventilator was specifically designed to deliver a constant gas volume (13), typically set to deliver a tidal volume of 250 μl for a 25 g mouse. The ventilator delivered 75% N_2 and 25% O_2 during normal life support, with the nitrogen replaced by HP ^{3}He for the imaging. For MCh delivery, the mice received a 2F catheter (Sherwood Medical, Tullamore, Ireland) in the jugular vein and MCh at a concentration of 80 μg/ml was administered by an infusion pump.

This work is divided into four distinct studies to demonstrate different aspects of the technique. We demonstrate the importance of normalization in a naïve C57BL/6 mouse given a “sham” MCh challenge (saline) by showing in a 2D time-dependent protocol in which difference mapping without normalization shows apparent reduction in ventilation, whereas normalization eliminates such false results. We then apply the normalized difference mapping method to a temporally resolved 2D dataset (2D + time) of an Ova-sensitized Balb/c mouse imaged during MCh challenge to reveal acute ventilation and airway caliber changes. We then apply the difference mapping method to 3D images acquired before and after MCh challenge in Ova-sensitized Balb/c mice, revealing more persistent ventilation changes. Finally, in an AJ mouse, we obtain MCh dose-response data consisting of 5 sets of 3D ventilation under the following conditions: baseline, after sham challenge, and after 50 μg/kg, 100 μg/kg, and 250 μg/kg MCh challenges. We use this data to show that the standard deviation of the difference map histogram increases linearly with MCh dose, suggesting that standard deviation may be a viable quantitative biomarker for evaluating asthma models.

Image Acquisition

Non-slice-selective coronal 2D images were acquired with field of view (FOV)=2.4 cm, using a 2D radial encoding sequence. Images employed a 132 μs hard excitation pulse, TR=5ms, TE=284 μs, BW=31.25 kHz, with 20 radial *k*-space views per breath, acquired with a variable flip angle to maintain constant magnetization with the final flip of 90°. Data acquisition continued for 12 s until 400 radial *k*-space views had been accumulated. Radial data was regridded on a Cartesian matrix of 128 × 128 and Fourier-transformed to yield images with a Nyquist-limited resolution of 187 × 187 μm^2.

High-resolution 3D images were acquired with a FOV of 2.0 cm in the coronal plane and 3.2 cm in the sagittal direction using 3D radial encoding (14). Images were acquired using a thick slab-selective excitation pulse, TR=5ms, TE=872 μs, BW=31.25 kHz, with 20 radial *k*-space views per breath, again incrementing the flip angle to maintain constant magnetization. Data acquisition continued over 5 minutes until 10,000 radial *k*-space views had been accumulated. Radial data was then reconstructed using a Non-Uniform Fast Fourier Transform (NUFFT)-

based reconstruction (15), and regridded on a Cartesian matrix of 128 × 128 × 32 to give images with a Nyquist-limited resolution of 157 × 157 × 1000 μm^3.

Hypolarized ^{3}He images were acquired at 64.8 MHz on a 2.0 T horizontal 18 cm clear bore magnet (Oxford Instruments, Oxford, UK) with shielded gradients (400 mT/m), controlled by a GE EXCITE 12M4 console (GE Healthcare, Milwaukee, WI). Further details regarding the imaging protocol, animal preparation, methacholine administration, and gas polarization are detailed in references (1) and (12).

Pre-Processing: Image Registration

2D and 3D images were visually inspected for significant changes at the edges to determine the need for image registration. 2D images acquired over a short time span did not show significant changes at the edges and hence they did not require registration. 3D images acquired over a longer period of time needed image registration to correct for some positional change, which was attributed to the waning effects of anesthetics.

Image registration was performed using the Image Registration Toolkit developed by Rueckert *et al.* (16). Initial registration used a rigid transformation to bring the images into the same coordinate space. Rigid, rather than non-rigid, registration was chosen because the latter could be confounded by ventilation defects that occur post-MCh. Registration used normalized mutual information as the cost function and linear interpolation was used to estimate intensities at non-integral pixel locations. A multi-resolution approach (17) was used to register the images starting at a lower resolution of 32 × 32 × 8 and successively increasing the resolution to the finest resolution of 128 × 128 × 32. At each resolution a deformation file was generated to serve as an initial estimate for the registration at the next finer resolution level. The source and target images were blurred at each resolution level, by specifying the radius of a Gaussian kernel, which increased from the lower to higher resolution levels.

Image Normalization

To normalize the pre- and post-MCh images prior to subtraction, we use the ^{3}He signal from the trachea as a calibration factor to turn images into fractional ^{3}He distribution maps that are independent of overall intensity. The ^{3}He signal intensity I_{vox} in any given voxel in the lung is directly related to its ^{3}He concentration, which in turn is related to ^{3}He volume V_{3He} delivered to it during each breath by

$$I_{vox}=\kappa\frac{V_{3He}}{V_{vox}} \tag{1.1}$$

where V_{vox} is the voxel volume, and κ is a proportionality constant. (This is true for our acquisition strategy because the final RF pulse applied during each breath is 90° and thus destroys all residual magnetization in the lung and avoids complex magnetization dynamics from previous breaths.) We know from basic physiology and previous studies that 100% of the ^{3}He in the trachea is replenished with each breath (11), and therefore voxels within the trachea follow $V_{3He}=V_{vox}$. Hence their intensity I_{trach} provides a solution for the proportionality constant of $\kappa=I_{trach}$. This intensity can then be used to normalize each pixel in the image according to

$$I_{norm}=\frac{I_{vox}}{I_{trach}}=\frac{V_{3He}}{V_{vox}}, \tag{1.2}$$

resulting in new intensities that will range from 0 to 1. Although, we do not explicitly validate this claim, these normalized intensities can be thought of as roughly the regional fractional ventilation parameter *r* defined by Denninger (11) and discussed in the introduction to this paper.

Rather than using only one pixel in the trachea for normalization, it is preferable to average the intensities from multiple pixels. This is done, as illustrated in Figure 1, by selecting a cylindrical region of diameter *D* and height *H* in the trachea and averaging the intensities of all pixels contained therein. While pixels within the interior of the trachea will be filled with pure ^{3}He, those at the edge may contain only a partial volume of ^{3}He. This partial volume effect must be corrected by including a geometric factor η, giving

$$\langle I_{trach}\rangle = \frac{\eta}{N_{trach}} \sum_{cyl} I_{trach}. \tag{1.3}$$

We calculate η by assuming the trachea to be a cylinder, in which case, it becomes simply the ratio of volumes of the 3D rectangular box of $D \times D \times H$ vs. that of a $D \times H$ cylinder, or $\eta = 4/\pi$. Furthermore, we can calculate N_{trach} according to the number of pixels in the 3D rectangle to give $N_{trach} = D^2 H/V_{vox}$. This gives a final value for the average trachea intensity of

$$\langle I_{trach}\rangle = \frac{4V_{vox}}{\pi D^2 H} \sum_{cyl} I_{trach} = \frac{V_{vox}}{V_{cyl}} \sum_{cyl} I_{trach} \tag{1.4}$$

An important technical consideration is that to use the ^{3}He signal from the trachea to normalize the images requires first the ability to visualize the trachea, and second that the trachea signal is directly representative of the ^{3}He spin density in a single breath. Therefore, these requirements demand very specific attention to the problem posed by signal attenuation induced by ^{3}He diffusion in the presence of imaging gradients. This issue is particularly acute at the microscopic resolution (high gradient strengths) used for mouse imaging and is further exacerbated by the nearly free diffusion of ^{3}He in the trachea. The problem received considerable attention from Johnson *et al.* (18) and later by Driehuys *et al.* (1), who showed that resolving small and large airways at high spatial resolution is made possible by employing a radial encoding sequence rather than more standard Cartesian sequences. Cartesian acquisitions can accumulate significant diffusion weighting as the trajectory goes to the edge of *k*-space and back. By contrast, center-out radial encoding sequences with short echo times (TE=284 μs) do not exhibit signal attenuation because the center of *k*-space is sampled before any gradient integral has been accumulated.

Image Analysis

All image analysis follows a standard protocol that is performed using an in-house MATLAB® (The MathWorks Inc., Natick, MA, USA) code that allows selection of a region within the trachea to estimate the calibration factor, applies the normalization, and creates difference maps.

The 2D datasets consisted of multiple images acquired at various time-points before and after the injection of MCh. Each image in the series was normalized using its own calibration factor and then divided by the pixel area to create a percent gas distribution map. The first normalized image in the series was the baseline image and was subtracted from all the remaining normalized images of the time series to generate a series of difference maps. For comparison,

thresholded images were also created, by retaining only pixels whose intensity exceeded 5-times the standard deviation of background (10).

For 2D difference maps, it is important to note that the percent gas volume change can be higher than 100%, since 2D datasets are anisotropic and can contain more or less lung in the direction perpendicular to the image plane. Thus, while the difference maps generated do not reflect absolute percent change in gas volume, the normalization and subtraction approach is still valid. In fact, a difference map series between the post- and pre-MCh challenge images can still be generated to show the regions of hypoventilation (<0 on difference map) and hyperventilation (>0 on difference map).

To normalize the 3D datasets, the volume was collapsed into a 2D coronal projection and an operator selected a cylindrical region in the trachea. This was carried out for both the pre- and post-MCh image volumes and this normalization step was used to render the images into ^{3}He percentage maps. These maps had a scale ranging from 0-to-100% representing no ventilation to complete ventilation. These maps could then be subtracted to create a slice-by-slice difference map with scale ranges from −100% to +100%, corresponding to a total loss of ventilation after MCh to complete restoration of ventilation. The difference maps were further quantified by plotting their histograms and calculating the SD of the distribution.

RESULTS

Figure 2 shows an analysis of selected frames from a 2D ^{3}He time-series acquired from a C57BL/6 mouse that was not injected with MCh. The figure shows a) the original images, b) threshold segmented images, c) difference maps without normalization, and d) difference maps with normalization. This animal should exhibit no ventilation changes and this is visually apparent in the ^{3}He images in Figure 2a and is effectively confirmed by the simple threshold segmentation technique shown in Figure 2b. However, difference maps created by directly subtracting the post-MCh images from the baseline image (shown in Figure 2c) seem to indicate that ventilation has been reduced, particularly towards the later frames at t=120s. These apparent ventilation changes are attributable to non-physiological factors, in this case likely from a slight reduction of ^{3}He volume delivery due to emptying of the ^{3}He bag. This effect is corrected by first normalizing the images before creating the difference map, as shown in Figure 2d. The normalized difference maps exhibit only residual non-zero signals that are within the standard deviation of noise in the images.

Figure 3 shows the normalized difference mapping technique applied to an ovalbumin-sensitized Balb/c mouse imaged under the 2D+time protocol. Figure 3a shows the original ^{3}He time series images that reveal airway narrowing (yellow arrows in left and right lung) with the subsequent recovery at t=120s (red arrows in left and right lung) as well as a focal loss of ventilation in the lower right lobe. The focal change (shown by ovals) is readily picked up in the threshold-segmented images (Figure 3b), but thresholding fails to detect the airway caliber changes or the more subtle residual hypoventilation at t=120s. By contrast, the normalized difference map reveals airway narrowing (yellow arrows), airway caliber recovery (red arrows), focal (oval), and diffuse changes in ventilation, as shown in Figure 3c.

Figure 4a shows selected slices from a 3D dataset of an ovalbumin-sensitized mouse imaged before the injection of MCh. Figure 4b shows the same slices from the mouse after it was challenged with 80 μg/kg of MCh. The images reveal increased ventilation in the upper left lung post-MCh and this effect is very clearly highlighted by the normalized difference map shown in Figure 4c, along with hyperintense signal in the large airways. The remainder of the lung exhibits subtle, diffuse hypoventilation.

Figure 5 shows 4 central slices from an A/J mouse scanned at different doses of MCh. Figure 5a shows the mouse lung images at baseline before the injection of MCh. Figure 5b shows the mouse lungs after a "sham" challenge obtained by injecting an equivalent volume of saline to a 250 μg/kg MCh challenge. The subsequent rows in Figure 5 show images captured at increasing MCh dose levels—Figure 5c (50 μg/kg), 5d (100 μg/kg), and 5e (250 μg/kg). For this study, an A/J mouse was chosen, because this strain is known to be inherently hyperresponsive (19) and hence, offers a useful and interesting test-bed. However, despite their hyperresponsiveness, A/J mice do not show complete airway closure (19) and therefore, provide a stringent test for image analysis. Indeed, inspection of the gray-scale images reveals some airway narrowing (arrows), but no obvious changes in ventilation, except for some hyperventilation noted in the apex of the right lung after 250 μg/kg MCh challenge (arrows).

Figure 6 a shows the same 4 pre-MCh slices from the AJ mouse of Figure 5a, while the remaining rows show the difference maps generated from the b) saline challenge, and the c) 50 μg/kg, d) 100 μg/kg, and e) 250 μg/kg MCh challenges. The difference maps created from saline challenge show very small deviations from baseline. Residual differences could stem from minor misregistration and noise. However, those difference maps created from images following actual MCh challenge clearly depict airway narrowing, regions of hypoventilation, and regions of compensatory hyperventilation caused by the constant volume ventilation used in these experiments. Moreover, all maps show a considerable heterogeneity to the gas distribution for increasing dose of MCh.

One way to quantify the difference maps shown in Figure 6, while retaining information uniquely generated from imaging, is to calculate the standard deviation (SD) of their histograms. For example, the histograms from the saline and 250 μg/kg MCh challenges are shown in Figure 7a and 7b. The SD from these histograms can be plotted as a function of MCh dose as shown in Figure 7c, which clearly demonstrates a trend towards increased SD as the MCh dose is increased.

DISCUSSION

We have demonstrated a technique to create a voxel-by-voxel map to quantitatively analyze regional changes in ventilation based on HP ^{3}He MRI. The method has three required steps: First, images must accurately depict the major airways so that they can serve to normalize the data. Secondly, images need to be registered to a common coordinate space to ensure that the difference maps are accurate. Finally, after registration and normalization, images can be used to generate a difference map that clearly depicts regions where ventilation has been altered by the MCh challenge. The method captures regional information about both focal and diffuse changes in ventilation, as well as narrowing of airways. Many of the changes apparent in the difference maps are not readily appreciated from visual inspection or simple threshold-based analysis.

The goal of our analysis technique is to provide a quantitative biomarker that differentiates treatment groups in a disease model. For imaging-based techniques, this requires the delicate balance of retaining the rich information afforded by 3D imaging, while collapsing this information to a single global metric of change. We have proposed use the standard deviation of the difference map histograms. The standard deviation changes appropriately with MCh dose, and encompasses much of the richness inherent in imaging.

The image normalization applied to generate difference maps requires the trachea to be visible in the HP ^{3}He images. This is possible, especially for small animal applications, only by using center-out radial imaging methods. The use of center-out radial imaging ensures the minimal loss of signal due to diffusion at the center of *k*-space. There will, however, be some diffusion-

induced signal loss at the periphery of the *k*-space, which may cause some signal loss at the edge of the trachea. However, the impact on calibration is minimal as this impacts only a very small fraction of the pixels selected for calibration.

One assumption of our method is that the trachea is a cylindrical volume. This may not be the case, especially when the placement of animal in the magnet is such that the trachea is not orthogonal to one of the imaging axes. This can be corrected by rotating the raw images such that the cylindrical assumption of the trachea is valid. However, this requires that no image reconstruction artifacts exist in the background, which are likely to overestimate the calibration factor.

The other assumption of this technique is that the imaging is performed at the same phase of the respiratory cycle and that the lung inflates to the same capacity during each breath. This is addressed by using a calibrated constant volume ventilator. While the use of a constant volume ventilator ensures the repeatability of the lung inflation, sometimes there are changes in the lung shape. These can be associated with slight shifts of the animal position resulting from temporarily reduced anesthetic depth. In such cases where a change in shape is observed, we have shown that pre- and post-MCh images can be registered (16) using an affine model before applying the normalized difference mapping technique.

Although the normalized difference mapping technique is developed for small animal applications, the technique can be applied to clinical studies. But, this will undoubtedly require image registration to align the images. A particular challenge for human subjects will be the reproducibility of the inhalation and consistent visibility of the trachea. To the extent that this is imperfect, the registration may have to rely on non-rigid registration algorithms. Such algorithms must be applied with care, in case they unintentionally remove real ventilation defects in the process. Such unintended removal of defects can likely be mitigated by using a landmark-based non-rigid registration, rather than the mutual information methods presented here. We are currently exploring landmark-based registration to compare mice with defects detected at baseline to normal control mice to permit application of this difference mapping method.

Acknowledgments

The authors are grateful to Gary Cofer for help with the MR coil and pulse sequences, Dr. Alexandra Badea for assistance with image registration, and Sally Zimney for assistance in preparing the manuscript. This work was performed at the Duke Center for In Vivo Microscopy, an NIH/NCRR National Biomedical Technology Research Center (P41 RR005959) and NCI Small Animal Imaging Resource Program (U24 CA092656), with additional support from NHLBI (R21 HL087094).

REFERENCES

1. Driehuys B, Walker JKL, Pollaro J, Cofer GP, Mistry NN, Schwartz DA, Johnson GA. 3He MRI in Mouse Models of Asthma. Magn Reson Med 2007;58:893–900. [PubMed: 17969115]
2. Whitehead GS, Walker JKL, Berman KG, Foster WM, Schwartz DA. Allergen-induced airway disease is mouse strain dependent. Am J Physiol Lung Cell Mol Physiol 2003;285:L32–L42. [PubMed: 12626335]
3. Glaab T, Taube C, Braun A, Mitzner W. Invasive and noninvasive methods for studying pulmonary function in mice. Respiratory Research 2007;8(1):63. [PubMed: 17868442]
4. Tattersfield AE, Keeping IM. Assessing change in airway caliber—measurement of airway resistance. Br J Clin Pharmacol 1979;8(4):307–319. [PubMed: 41547]
5. Simcock DE, Kanabar B, Clarke GW, O'Connor BJ, Lee TH, Hirst SJ. Proangiogenic Activity in Bronchoalveolar Lavage Fluid from Patients with Asthma. Am J Respir Crit Care Med 2007;176:146–153. [PubMed: 17463417]

6. Stevenson EC, Turner G, Heaney LG, Schock BC, Taylor R, Gallagher T, Ennis M, Shields MD. Bronchoalveolar lavage findings suggest two different forms of childhood asthma. Clinical and Experimental Allergy 1997;27:1027–1035. [PubMed: 9678834]
7. Altes TA, Powers PL, Knight-Scott J, Rakes G, Platts-Mills TAE, de Lange EE, Alford BA, Mugler JP III, Brookeman JR. Hyperpolarized 3He MR Lung Ventilation Imaging in Asthmatics: Preliminary Findings. J Magn Reson Imaging 2001;13:378–384. [PubMed: 11241810]
8. de Lange EE, Altes TA, Patrie JT, Parmar J, Brookeman JR, Mugler JP III, Platts-Mills TAE. The variability of regional airflow obstruction within the lungs of patients with asthma: Assessment with hyperpolarized helium-3 magnetic resonance imaging. J Allergy Clin Immunol 2007;119:1072–1078. [PubMed: 17353032]
9. Samee S, Altes TA, Powers PL, de Lange EE, Knight-Scott J, Rakes G, Mugler JP III, Ciambotti J, Alford BA, Brookeman JR. Imaging the lungs in asthmatic patients by using hyperpolarized helium-3 magnetic resonance: Assessment of response to methacholine and exercise challenge. J Allergy Clin Immunol 2003;111:1205–1211. [PubMed: 12789218]
10. Woodhouse N, Wild JM, Paley MNJ, Fichele S, Said Z, Swift AJ, van Beek EJR. Combined Helium-3/Proton Magnetic Resonance Imaging Measurement of Ventilated Lung Volumes in Smokers Compared to Never-Smokers. J Magn Reson Imaging 2005;21:365–369. [PubMed: 15779032]
11. Deninger AJ, Mansson S, Petersson JS, Pettersson G, Magnusson P, Svensson J, Fridlund B, Hansson G, Erjefeldt I, Wollmer P, Golman K. Quantitative measurement of regional lung ventilation using 3He MRI. Magn Reson Med 2002;48:223–232. [PubMed: 12210930]
12. Thomas AC, Potts EN, Chen BT, Slipetz DM, Foster WM, Driehuys B. A robust protocol for regional evaluation of methacholine challenge in mouse models of allergic asthma using hyperpolarized 3He MRI. NMR Biomed 2009;22(5):502–515. [PubMed: 19204996]
13. Chen BT, Yordanov AT, Johnson GA. Ventilation-Synchronous Magnetic Resonance Microscopy of Pulmonary Structure and Ventilation in Mice. Magn Reson Med 2005;53:69–75. [PubMed: 15690504]
14. Shattuck MD, Gewalt SL, Glover GH, Hedlund LW, Johnson GA. MR microimaging of the lung using volume projection encoding. Magn Reson Med 1997;38:938–942. [PubMed: 9402195]
15. Song JY, Liu YH, Gewalt SL, Cofer G, Johnson GA, Liu QH. Least-Square NUFFT Methods Applied to 2-D and 3-D Radially Encoded MR Image Reconstruction. IEEE Transactions on Biomedical Engineering 2009;56(4):1134–1142. [PubMed: 19174334]
16. Rueckert D, Sonoda LI, Hayes C, Hill DLG, Leach MO, Hawkes DJ. Non- rigid registration using free-form deformations: Application to breast MR images. IEEE Transactions on Medical Imaging 1999;18(8):712–721. [PubMed: 10534053]
17. Studholme C, Hill DLG, Hawkes DJ. An Overlap Invariant Entropy Measure of 3D Medical Image Alignment. Pattern Recognition 1999;32(1):71–86.
18. Johnson GA, Cates GD, Chen XJ, Cofer GP, Driehuys B, Happer W, Hedlund LW, Saam B, Shattuck MD, Swartz J. Dynamics of magnetization in hyperpolarized gas MRI of the lung. Magn Reson Med 1997;38(1):66–71. [PubMed: 9211381]
19. Wagers SS, Haverkamp HC, Bates JHT, Norton RJ, Thompson-Figueroa JA, Sullivan MJ, Irvin CG. Intrinsic and antigen-induced airway hyperresponsiveness are the result of diverse physiological mechanisms. J Appl Physiol 2007;102:221–230. [PubMed: 17008432]

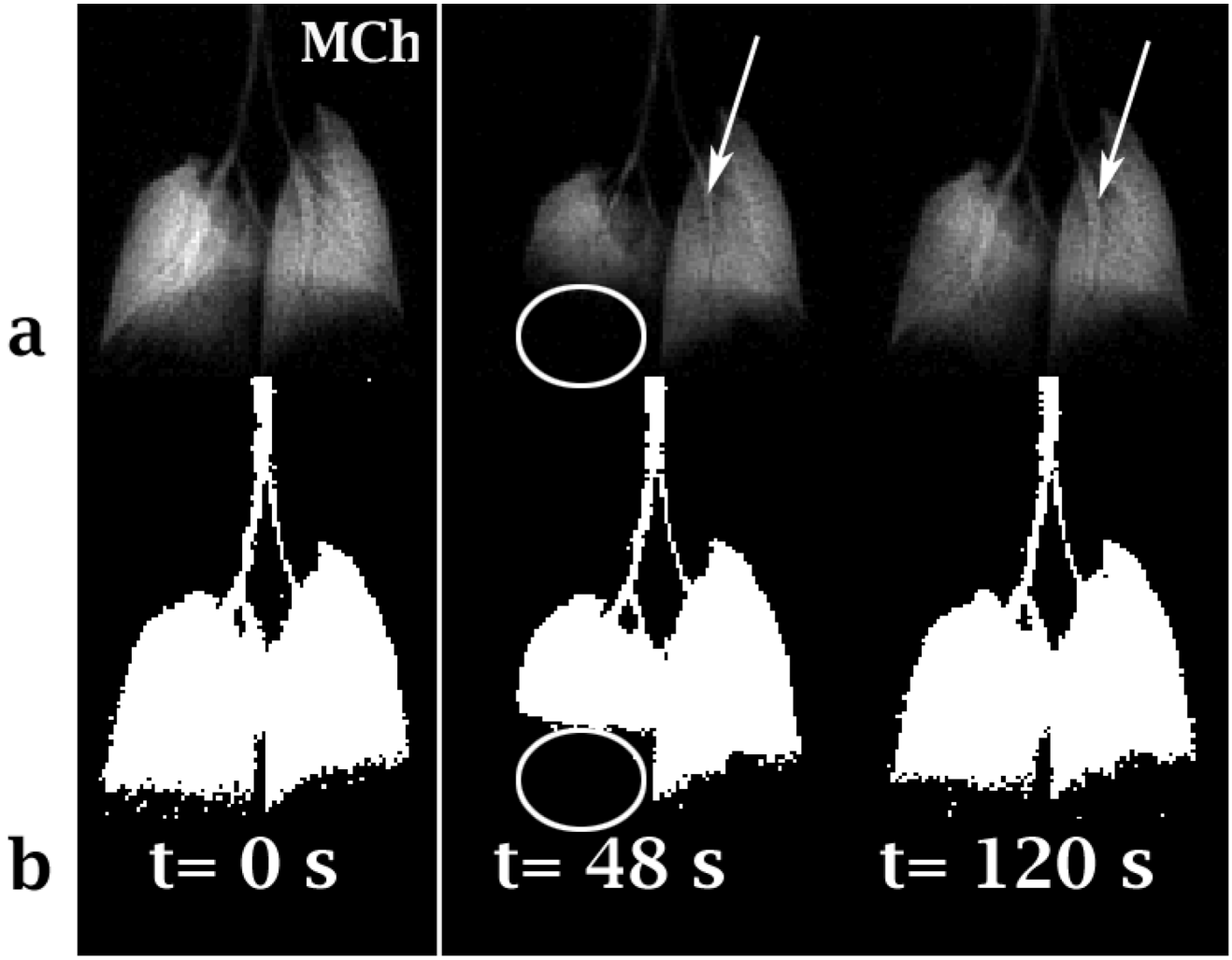

Figure 1.
A cylindrical selection in the trachea is used to normalize the signal intensity in each image, so that variations from signal decay resulting from non-physiological factors such as loss of polarization can be accounted for.

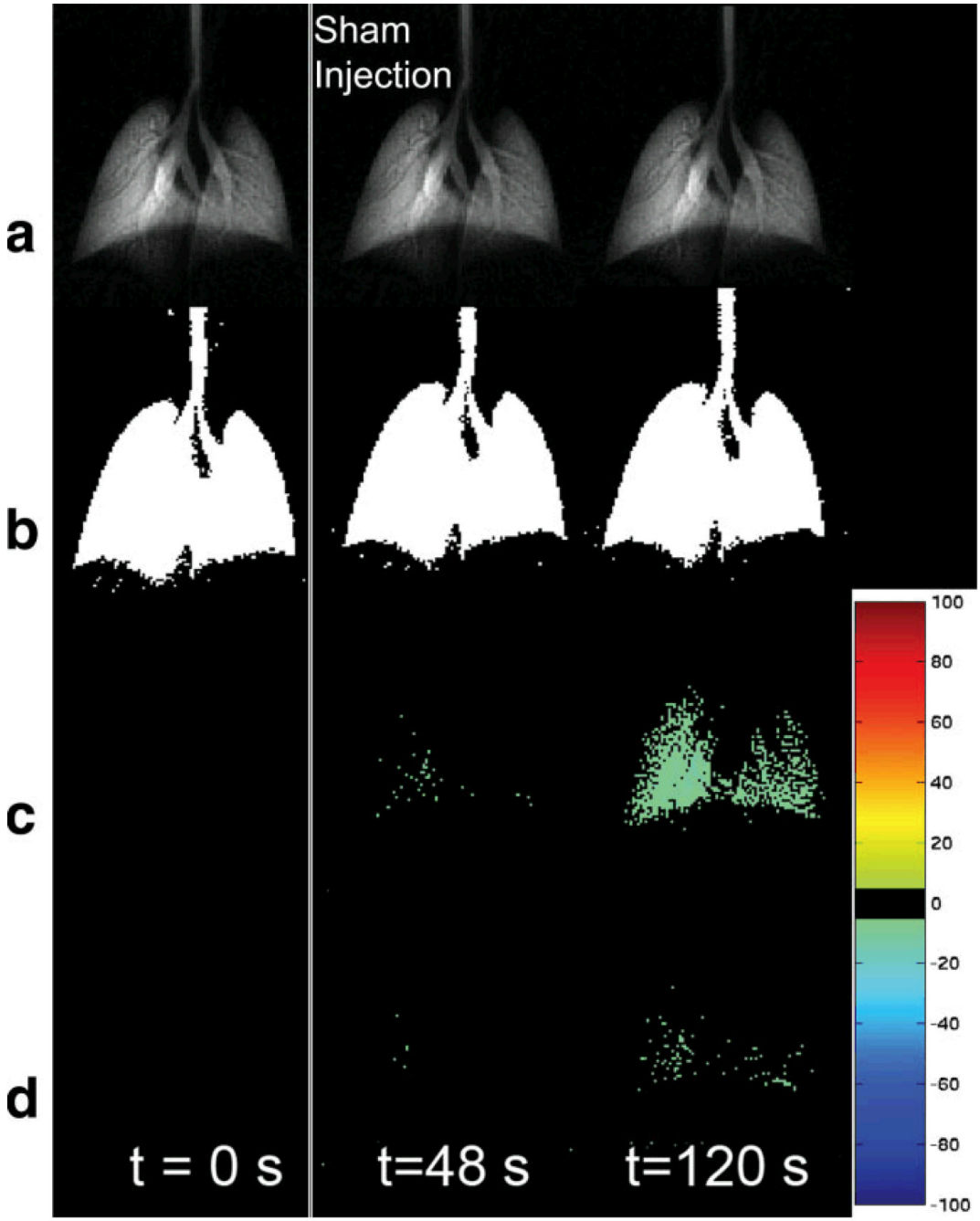

Figure 2.

a) Baseline time-series ^{3}He images acquired without MCh challenge from a C57BL/6 naïve mouse at three different time points; b) threshold segmented ventilation images showing no change in ventilation; c) difference maps created from time-series of images; d) normalized difference maps showing close to 0% change in all regions of the lung even at t=120s.

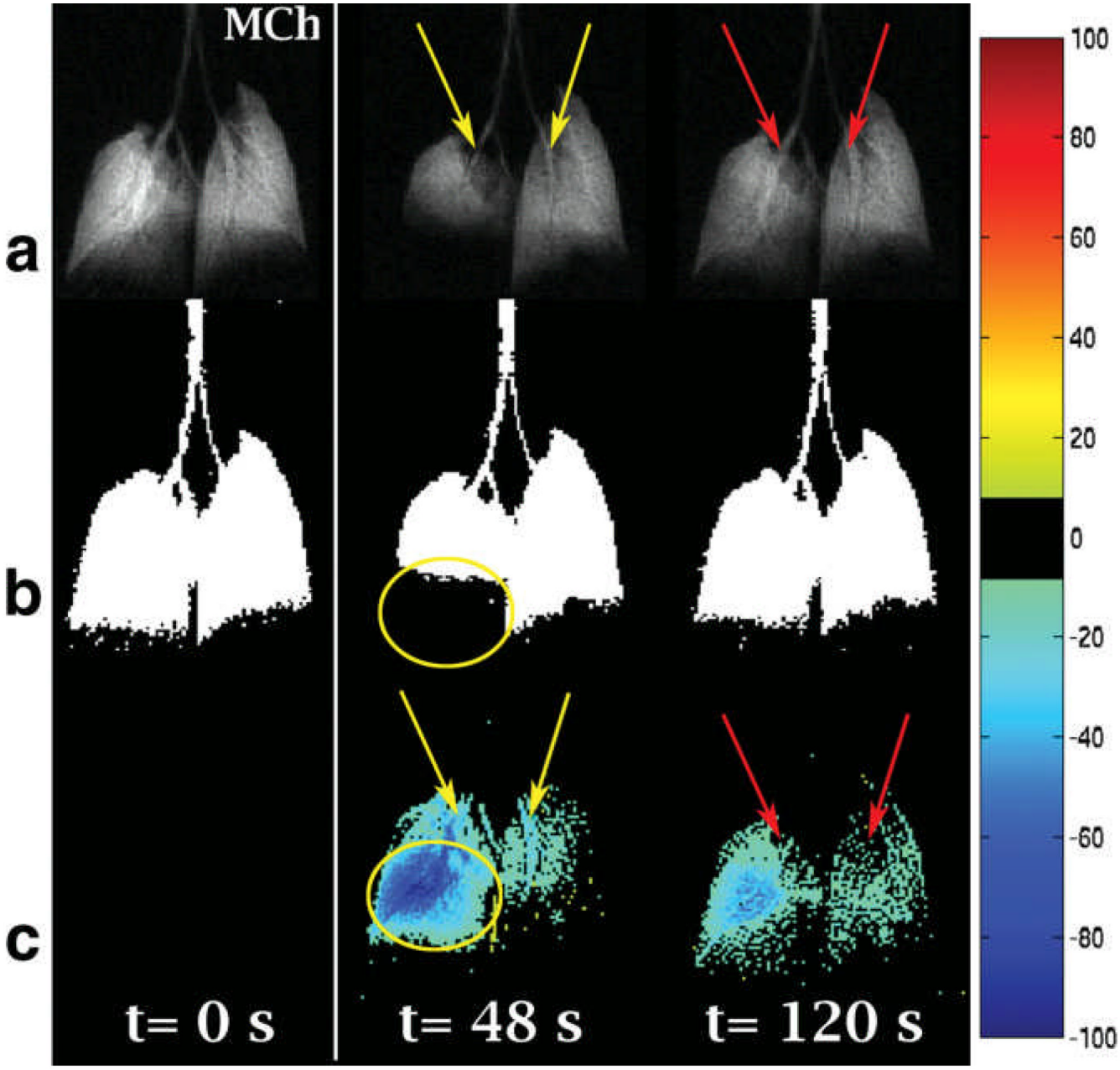

Figure 3.

a) Baseline time-series ^{3}He images acquired from an ovalbumin-sensitized mouse showing airway narrowing (yellow arrows) and focal ventilation change; b) threshold segmented ventilation images pick up focal change (oval); c) difference maps shows airway narrowing (yellow arrows), airway recovery (red arrows) focal change (oval), and diffuse changes in the whole lung.

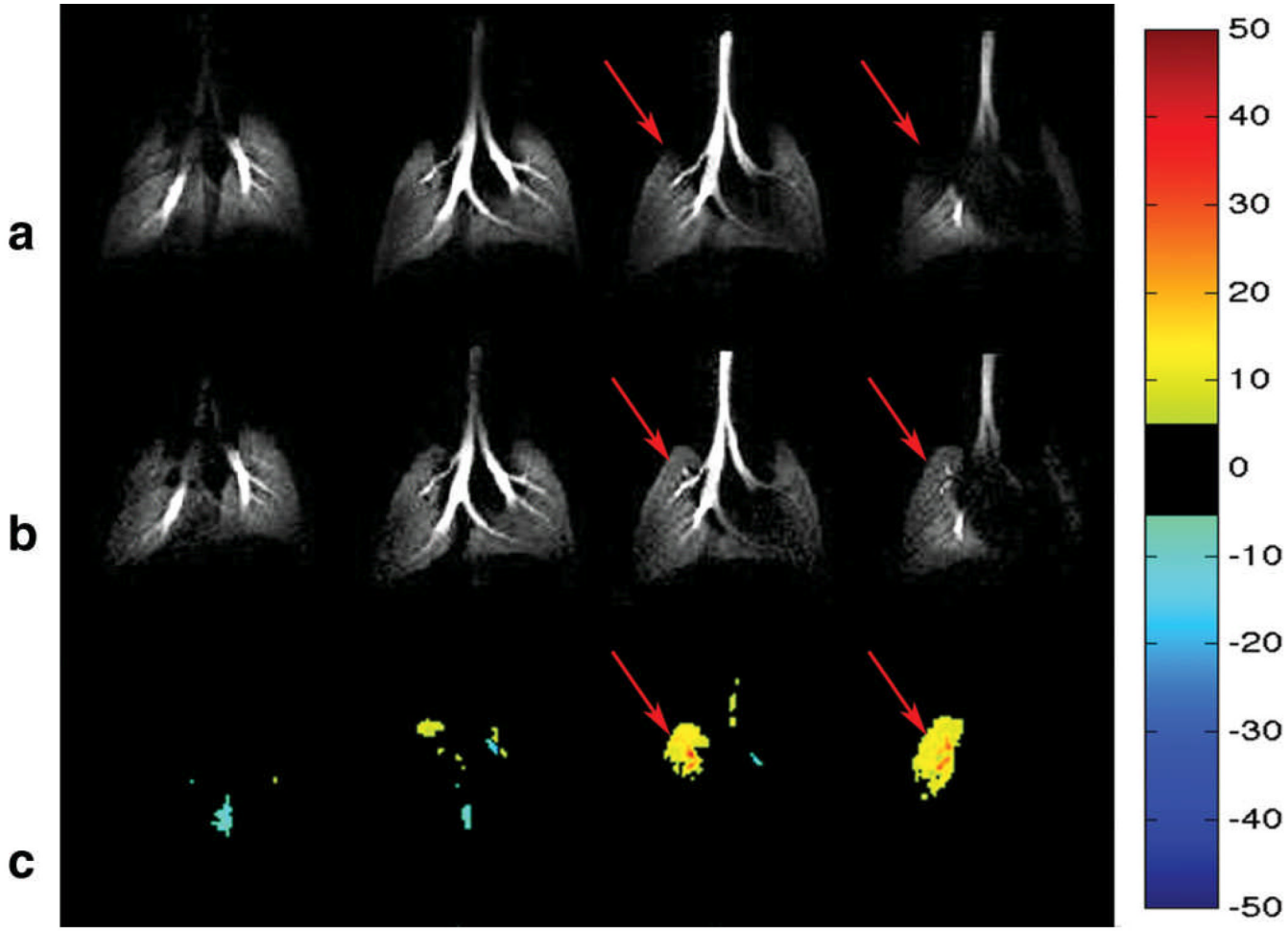

Figure 4.

a) Pre-MCh challenge ^{3}He image slices from an ovalbumin-sensitized mouse. b) Post-MCh challenge following 80 μg/kg of MCh. c) Difference maps created from ^{3}He percentage maps; Note the region of hyperventilation observed in the upper left lobe (arrow), whereas the remaining regions show subtle hypoventilation in the peripheral region of the lung.

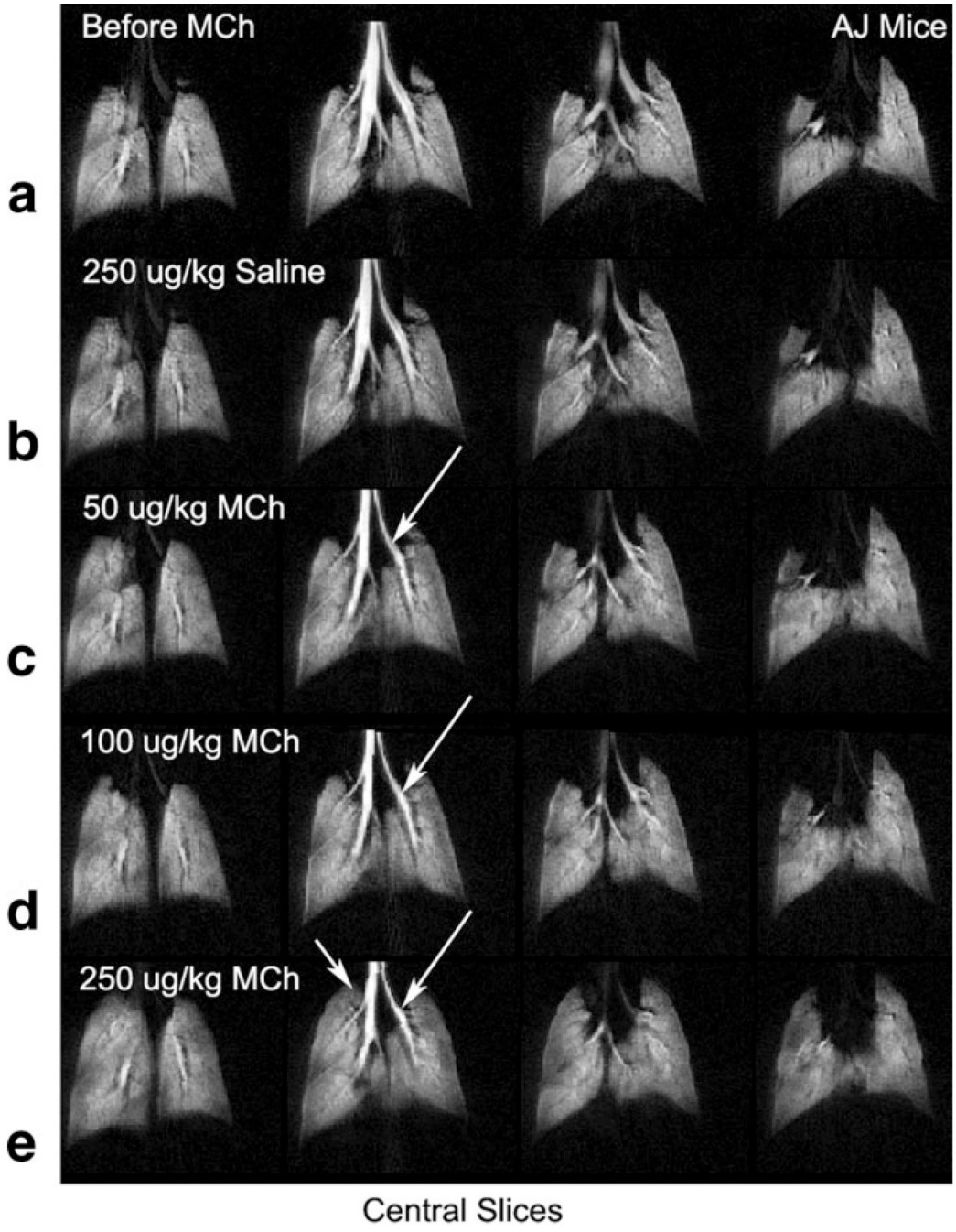

Figure 5.

Central slices from a 3D ^{3}He datasets collected from an AJ mouse imaged a) before the injection of MCh, b) after the injection of 250 μg/kg of saline, c) 50 μg/kg, d) 100 μg/kg, and e) 250 μg/kg of MCh. This mouse strain, while hyperresponsive, exhibits no airway closure and presents a significant challenge for simple visual image analysis.

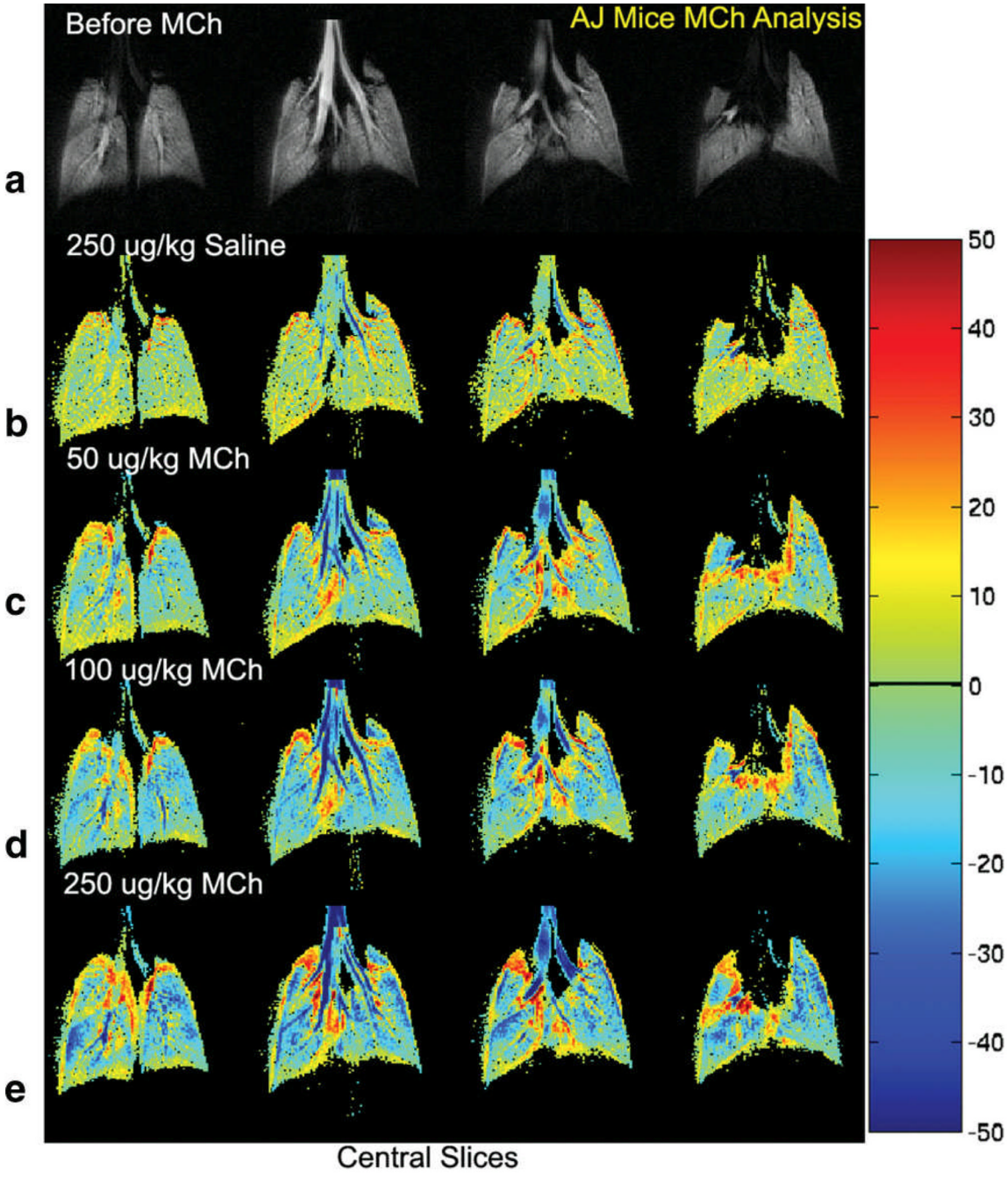

Figure 6.
Baseline ^{3}He images and difference maps created from the central slices from the images shown in Figure 5. Difference maps show increased heterogeneity (larger regions showing hypoventilation and hyperventilation) with higher dose of MCh.

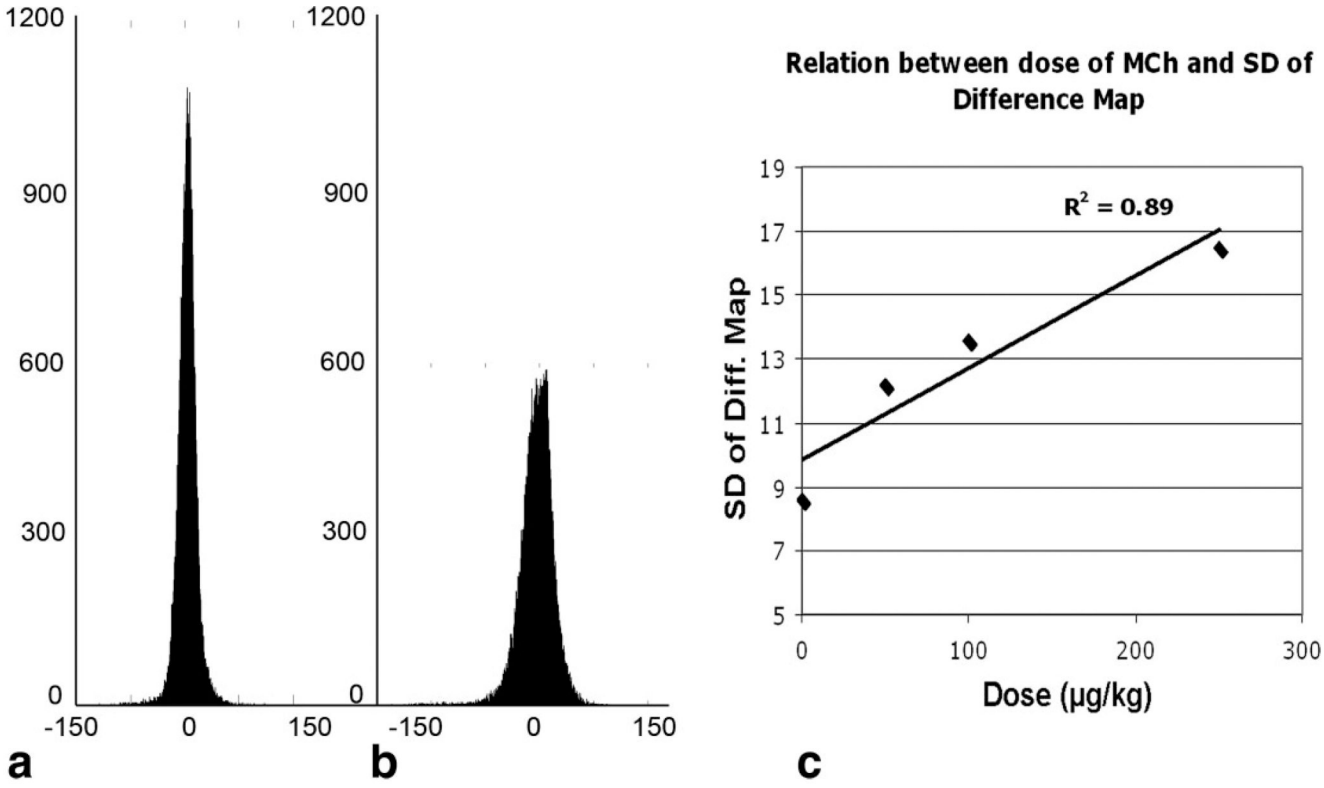

Figure 7.

a) Histogram from saline challenge, b) histogram from 250 µg/kg MCh challenge, and c) plot of standard deviation (SD) (a.u.) of difference map shows an increasing trend for higher dose of MCh.